Electrophysiological Characterization of iPSC-derived Cortical Neurons Using Automated Patch Clamp

Kadla R. Rosholm[1], Ivy Pin-Fang Chen[3], Daniel R. Sauter[2], Anders Lindqvist[1], Taylor E. Forman[3], Sean A. Dwyer[3], Cindy Yang[3], Elizabeth D. Buttermore[3]

1. Sophion Bioscience A/S, Baltorpvej 154, 2750 Ballerup – Denmark
2. Sophion Bioscience Inc., 400 Trade Center Drive, Suite 6900, Woburn, MA 01801 – United States
3. Human Neuron Core, Translational Neuroscience Center, Boston Children's Hospital, Boston, MA – United States

Introduction

Human induced pluripotent stem cells (hiPSCs) can be differentiated into many cell types, including neurons and cardiomyocytes, and therefore constitute a novel way to model human diseases[1]. However, hiPSC-based applications are often challenged by the variability among differentiation batches, even when using iPSC lines originating from a single donor, and by heterogeneity among specific cell types derived from iPSCs[2]. Here we demonstrate the application of high throughput electrophysiological measurements, using our automated patch clamp (APC) platform, Qube 384, for characterization of iPSC-derived cortical neurons.

Generic cortical neurons were differentiated from iPSCs using small molecules under dual-SMAD inhibition conditions[3]. The cells were handled and differentiated in parallel and a total of three independent differentiation batches were carried out. We conducted an electrophysiological analysis of the endogenous ion channel expression in the three different batches of iPSC neurons. In agreement with sequencing data, the measurements revealed a good reproducibility between the three iPSC batches with 60% - 70% of the investigated cells expressing voltage gated Na+ (Nav) channels and 60% - 80% expressing voltage gated K^+ (Kv) channels. Furthermore, filtering the measurements for the currents of interest, allowed a thorough biophysical and pharmacological investigation of the individual ion channels.

Finally, we compared iPSC-derived neurons from a patient (proband) carrying a missense mutation in cyclin-dependent kinase-like 5 (CDKL5) (c.871T>C, p.Cys291Arg), who was clinically diagnosed to present with classic CDKL5 Deficiency Disorder (CDD), with cells derived from an isogenic control. Using immunostaining, whole transcriptome analysis, and electrophysiological measurements we found that proband neurons were larger and had a more immature morphology, suggesting that they do not differentiate as efficiently as the control neurons.

Material and Methods

Cell culture

Mixed cortical neurons were differentiated using dual SMAD inhibition to generate neural progenitors, then neuronal media supplemented with growth factors was added to mature the progenitors into neurons. Five weeks post neural induction, neurons were dissociated and either re-plated or cryopreserved for experiments later. Cells for imaging were fixed 24 hours after re-plating.

The proband neurons were from a patient carrying a missense mutation in CDKL5 (c.871T>C, p.Cys291Arg), who was clinically diagnosed to present with classic CDD phenotypes, including refractory epilepsy and global developmental delay. The control was an isogenic control with the patient's mutation corrected through CRISPSR/Cas9 genome editing.

Neurons for APC were thawed and differentiated for an additional 3 weeks. After reaching 8 weeks post neural induction the culture medium was removed, and the cells were washed x2 in PBS and harvested using 2 mL Accumax™ per T25 cell flask (incubate 7 min at 37°C). Subsequently, 6 mL culture medium was added, and the cells were spun down (4 min, 150 x g) and resuspended in extracellular solution to achieve the required cell density.

Imaging

Neurons were plated at a density of 20K neurons per well and fixed 24 hours after plating. Fixed cells were immunostained with antibodies targeting Tuj1, MAP2, and PAX6. Cells were imaged using the ImageXpress Micro Confocal from Molecular Devices using a 10X objective. All cells were imaged using the same exposure times across wells and conditions.

Sequencing

For sequencing experiments, cells were collected directly into buffer RLT as part of the Qiagen RNeasy Kit. After RNA isolation, reverse transcription was completed with ThermoFisher's SuperScript VILO and libraries were prepped using ThermoFisher's Ion AmpliSeq Transcriptome Human Gene Expression Kit and library prep on the Ion Chef. Templating was also completed on the Ion Chef and loaded chips were sequenced on the Ion Torrent. TAC software was used to compare replicate samples and generate graphs. DAVID gene ontology analysis was completed to analyze pathways affected in probands neurons, compared with controls.

Electrophysiology measurements

Solutions: Extracellular solution (mM): 2 $CaCl_2$, 1 $MgCl_2$, 10 HEPES, 4 KCl, 145 NaCl, 10 Glucose, pH = 7.4 with NaOH, Osmolarity =305 mOsm with sucrose. Intracellular solution (mM): 120 KF, 20 KCl, 10 HEPES, 10 EGTA, pH = 7.2 with KOH, Osmolarity 300 mOsm with sucrose. **Voltage protocols**: The voltage step protocol consisted of a 500 ms pre-step at -120 mV followed by 500 ms voltage steps from -90 mV to + 120 mV (ΔV = 5 mV). **Analysis**: Cell quality filter criteria: The experiments were initially filtered based on the quality of the seal (membrane resistance R_{mem} > 500 MΩ) and size of the cells (cell capacitance C_{cell} > 1.5 pF) as well as manual inspection.

Imaging

Control neurons reveal the presence of Tuj1-positive and MAP2-positive cells with short neurites 24 hours after plating. CDKL5 proband neurons reveal more immature morphology, with large neural rosettes still present and Tuj1-positive neurons just beginning to emerge from the rosettes. In addition, quantification of cell numbers revealed an increase in PAX6-positive cells in proband cultures, a marker of neural progenitors rather than mature neurons. These data suggest that the probands neurons did not differentiate as efficiently as the control neurons.

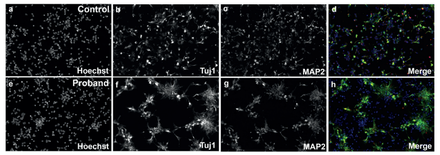

Fig. 1: Representative images of control and CDKL5 proband iPSC-derived neurons. (a-d) Control neurons stained with Hoechst stain (a), Tuj1 (b), MAP2 (c), and merged (d) reveal the presence of Tuj1-positive and MAP2-positive cells. (e-h) CDKL5 proband neurons stained with Hoechst stain (e), Tuj1 (f), MAP2 (g), and merged (h) reveal the presence of neural rosettes with a few neurons surrounding them.

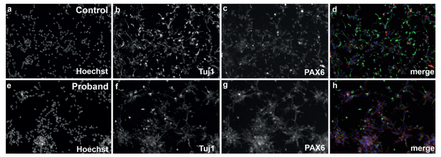

Fig. 2: Representative images of control and CDKL5 proband iPSC-derived neurons. (a-d) Control neurons stained with Hoechst (a), Tuj1 (b), PAX6 (c), and merged (d) reveal the presence of Tuj1-positive and PAX6-positive cells. (e-h) CDKL5 proband neurons stained with Hoechst (e), Tuj1 (f), PAX6 (g), and merged (h) reveal the presence of PAX6-positive neural rosettes with a few neurons surrounding them.

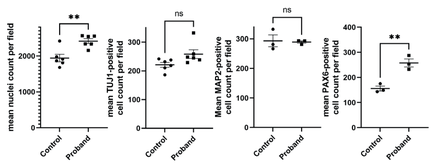

Fig. 3: Quantification of high content imaging reveals increased number of progenitors in proband cultures. (a) quantification of the number of nuclei in control versus proband cultures reveals an increase in cells in the CDKL5 proband cultures. (b-c) Quantification of the number of Tuj1-positive (b) and MAP2-positive (c) cells did not reveal significant differences between the genotypes. (d) Quantification of PAX6-positive cells revealed an increase in progenitor-like cells in CDKL5 proband cultures, compared with healthy controls, suggesting these cells have not fully differentiated at the same time-point. **= $p < 0.005$.

Sequencing analysis

Mixed cortical neurons derived from CDKL5 patient iPSCs or CRISPR-corrected iPSCs were collected at 5 weeks for RNA processing. Isolated RNA was sequenced using AmpliSeq™ technology, which resulted in gene expression level readouts from triplicate differentiations of each line. Genes that were either 1.2-fold (or more) increased or decreased in the probands, compared to the control with p-value < 0.05, were entered into DAVID gene ontology platform. This analysis revealed the following changes:

- Disrupted synaptic machinery
  - GRIN2A and DISC1 each 2-fold increased in proband vs CRISPR corrected
  - GRIA4 decreased and GRIK4 increased
  - Several cholinergic receptor subunits increased 1.5-fold
  - GABBR2 increased 2.5-fold
- Disrupted kinase function is #1 annotation cluster on DAVID
  - Several CDK family members, MAPK family members, PKC family members
- Sodium channels:
  - SCN5A is 1.7-fold decreased in proband
  - In general, in these neurons, SCN3B and SCN2A are most highly expressed, followed by SCN9A, SCN8A, SCN7A, SCN3A, and SCN2B
- Potassium channels:
  - decreased in proband
  - KCNG1, KCNK10, KCNH3 increased in proband
  - Many of the potassium channel isoforms are expressed in these neurons (too many to list here), including highest levels of KCNQ2 and KCNH2

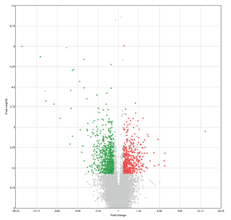

Fig. 4: Volcano plot clustering of genes up or down regulated in CDKL5 (proband) neurons compared to control neurons. This plot reveals the fold change (x-axis) and p-value (y-axis) of genes upregulated (red) and downregulated (green) in the probands neurons, compared to healthy control neurons.

Automated patch clamp

Experiment setup:

hiPSC derived cell lines are expensive and it is therefore of interest to limit cell consumption as much as possible. For that reason, we used a cell transfer plate (CTP), which allowed us to use small cell volumes (down to 170 µL) and to test several cell clones in parallel. Another challenge of hiPSC derived cells is that they typically display quite heterogeneous current expression. This might be due to different maturation states, different cell types or natural variation. In automated patch clamp (APC) currents are recorded from a large number of cells in parallel. This makes APC well suited to characterize cell populations and identify subpopulations.

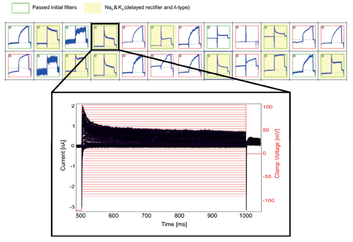

Fig. 5: Quality control filters allow selection of cells expressing the channels of interest. Top: Cut-out of the measurement plate (QChip) view showing 24 of 384 experiments. Red and green borders correspond to experiments that failed and passed, respectively, the initial filter criteria (R_{mem} > 500 MΩ, C_{cell} > 1.5 pF). The experiments highlighted in yellow passed filter criteria for Na$_v$ and K$_v$ currents. Bottom: Example current trace from a neuron, expressing Na$_v$ channels and a mixture of delayed rectifier and A-type K$_v$ channels.

Success rates

To further limit cell use, we identified the minimum cell density required to reach satisfactory success rates. The percentage experiments that passed the cell quality success criteria were plotted as a function of iPSC neuron suspension density (see Figure 6). The individual data points were quite scattered, however binning (red data points, N = 6 or 7) revealed an overall decrease in success rates at low cell densities. We found that the neuron density should be above 0.8 million per mL in order to yield satisfactory success rates.

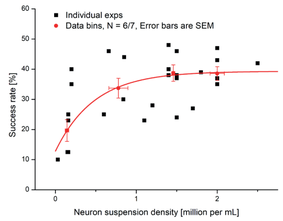

Fig. 6: Experiment success rate as a function of iPSC neuron density. Individual data points (black) were binned (red data points, N = 6 or 7) to visualize the trend in the data. Error bars are SEM.

Ion channel expression

The most abundant voltage-gated Na^+ (Na$_v$) channels and voltage-gated K^+ (K$_v$) channels in cortical neurons are[4,5]: Na$_v$1.1, Na$_v$1.2, Na$_v$1.6 and K$_v$1.1, K$_v$2, K$_v$3, K$_v$7.2/K$_v$7.3 (delayed rectifier), K$_v$4 (A-type). To compare ion-channel expression across three different batches from the same donor, the experiments were filtered to identify Na$_v$ or K$_v$ channels, and the percentage of cells with expression of the individual ion channels was displayed. The K$_v$ expressing cells were further sorted to identify the neurons expressing A-type K$_v$ channels.

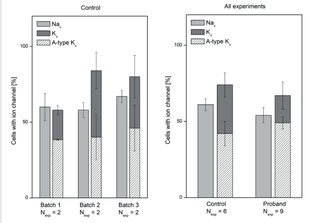

Fig. 7: The ion channel expression was reproducible between batches and between control and proband samples. The percentage (average ± SEM) of investigated cells containing Na$_v$ and K$_v$ were displayed for three different differentiation batches of the control cell line (left) and for the control and proband (right). Of the cells expressing K$_v$ channels, the percentage of K$_v$ expressing cells also having A-type K$_v$ currents are displayed on top (pattern). No significant differences were observed, neither between the three batches nor between the control and proband cell lines.

Ion channel analysis

Na$_v$ analysis

In agreement with literature, biophysical evaluation of the Na$_v$ currents indicate that only terodotoxin (TTX)-sensitive Na$_v$ channels (i.e. Na$_v$1.1, Na$_v$1.2, Na$_v$1.6) are present in the neurons (figure 11). Literature values of $V_{½}$ of activation/inactivation values are listed in Table 1. The extracted values are close to literature values for Na$_v$1.2, suggesting that this is the predominant Na$_v$ channel in the neurons. This could indicate that the majority of the neurons are excitatory and that they are not mature enough to express high levels of Na$_v$1.6.

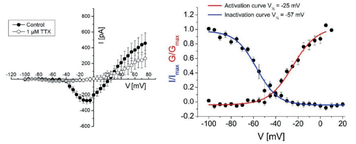

Fig. 11: Biophysical and pharmacological evaluation of Na$_v$ currents in control iPSC neurons confirms the presence of TTX-sensitive Na$_v$ channels with activation/inactivation characteristics indicative of Na$_v$1.2. Left: Average Na$_v$ current versus step voltage for control neurons before (black data points) and after (white data points) application of 1 µM TTX. N_{cells} = 65. Right: Na$_v$ conductance (G normalized to G_{max}, red) and inactivation current (I normalized to I_{max}, blue) versus step voltage. Boltzmann fits to the data were used to extract $V_{½}$ values of activation and inactivation, respectively. N_{cells} = 75.

Table 1: Literature values – V½ of activation/inactivation for Nav1.1, Nav1.2, Nav1.6.

Subtype	Steady-state slow inactivation	Activation
	$V_{½}$ [mV]	V½ [mV]
Na$_v$1.1	-72[8]	-33[8]
Na$_v$1.2	-53[9]	-24[9]
Na$_v$1.6	-72[10]	-29[10]

K$_v$ analysis

The K$_v$ steady state current was blocked by addition of 1 mM 4-aminopyridine (4-AP) (Figure 12).

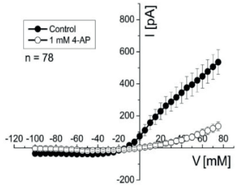

Fig. 12: Pharmacological evaluation of K$_v$ currents in control iPSC cortical neurons confirms the presence of K$_v$ channels. Left: Average K$_v$ current versus step voltage for control neurons before (black data points) and after (white data points) application of 1 mM 4-AP (TTX). N_{cells} = 78.

Conclusion

In summary, we here show several applications of APC for characterizing and investigating iPSC cortical neurons.

Parallel measurements of 384 neurons per measurement plate allowed us to compare ion channel expression (Na$_v$ and K$_v$) across three differentiation batches from the same donor, as well as between CDKL5 proband and isogenic control. We found Na$_v$ currents in 60% - 70% of the neurons and K$_v$ channels in 60% - 80% of the neurons with no significant difference between the samples.

Biophysical and pharmacological evaluation identified the primary Na$_v$ channel as Na$_v$1.2, indicating that the majority of the neurons are excitatory and that they are not mature enough to express high levels of Na$_v$1.6. In about 50% of K$_v$ expressing cells, the current displayed a mixture of delayed rectifier and A-type kinetics and showed a 80% block by compounds validating that only a minor part of the current was caused by leak.

Finally, we identified a subpopulation of mature neurons containing both Na$_v$ and K$_v$ (delayed rectifier and A-type) channels) for comparison of CDKL5 proband and isogenic control. Imaging, sequencing and APC data suggest that proband neurons are larger and more immature than control neurons, and might display small differences in K$_v$ channel expression.

Electrophysiological comparison of CDKL5 proband and control iPSC neurons:

The measurements were filtered to include only neurons expressing both voltage-gated Na$_v$ and K$_v$ channels, which is a sign of maturity. The membrane resistance (R_{mem}), cell capacitance (C_{cell}) and resting membrane potential (RMP) were compared between the proband and isogenic control.

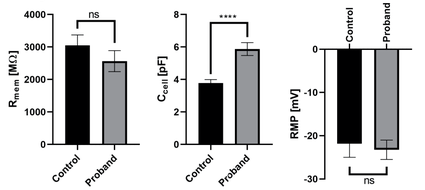

Fig. 8: Measurement of cell properties reveal a significant increase in cell size in proband cultures. R_{mem}, C_{cell} and RMP values were compared compared for control (N_{cells} = 85) and proband (N_{cells} = 69) neurons. The only significant difference observed was an increase in cell capacitance, and thus cell size, observed for the proband neurons (**** = p < 0.0001). This is in agreement with the observation that proband neurons are more immature than control neurons. Note that the RMP is elevated (~ -20 mV) as compared to expected values (~ -70 mV!). This could be due to the cells being in standard whole-cell conformation or that they lack a leak K^+ current (Kir or K2P) that could hyperpolarize the RMP[7].

Plotting the Na$_v$ current-voltage relationship did not reveal any significant differences between proband and control neurons (figure 9). However, comparing peak and steady-state current of K$_v$ channels in proband and control, showed a small but significant decrease in the steady-state current (figure 10). This is in agreement with sequencing results showing differences in K$_v$ channel expression.

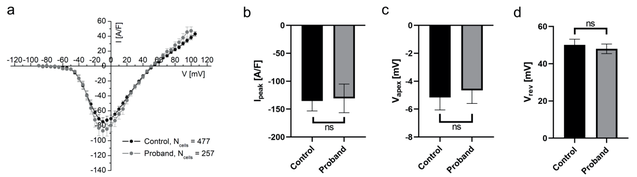

Fig. 9: Biophysical analysis of Na$_v$ currents in cortical neurons do not reveal any significant differences between CDKL5 proband and isogenic control neurons. a) The normalized Na$_v$ current-voltage relationship was plotted for control (N_{cells} = 477) and proband (N_{cells} = 257) neurons, respectively. b-d) Neurons that contained both Na$_v$ and K$_v$ channels were further analyzed to compare the normalized Na$_v$ peak current (I_{peak}), the voltage at current apex (V_{apex}) and reversal potential (V_{rev}). No significant differences were quantified between control (N_{cells} = 85) and proband (N_{cells} = 69) neurons. Bars are average ± SEM.

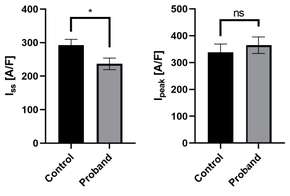

Fig. 10: Biophysical analysis of K$_v$ currents in cortical neurons reveal a small difference in the current from delayed rectifier K$_v$ channels. The steady-state current (I_s) and peak current (I_{peak}) were compared for control (N_{cells} = 85) and proband (N_{cells} = 69) neurons. The data showed a small, but significant decrease in I_{ss}, indicating a decreased expression of delayed rectifier K$_v$ channels. This observation is in agreement with sequencing data showing differences in the expression of several K$_v$ channel subunits. Bars are average ± SEM. * = p < 0.05.

References

1. Ko, H. C. & Gelb, B. D. Concise Review: Drug Discovery in the Age of the Induced Pluripotent Stem Cell. Stem Cells Transl. Med. 3, 500–509 (2014).
2. Thiry, L., Hamel, R., Pluchino, S. & Stifani, S. N EUROSCIENCE Characterization of Human iPSC-derived Spinal Motor Neurons by Single-cell RNA Sequencing. 450, 57–70 (2020).
3. Qi, Y. et al. Combined small-molecule inhibition accelerates the derivation of functional, early-born, cortical neurons from human pluripotent stem cells. 35, 154–163 (2017).
4. Child, N. D. & Benarroch, E. E. Differential distribution of voltage-gated ion channels in cortical neurons: Implications for epilepsy. Neurology 82, 989–999 (2014).
5. Duménieu, M., Oulé, M., Kreutz, M. R. & Lopez-Rojas, J. The segregated expression of voltage-gated potassium and sodium channels in neuronal membranes: Functional implications and regulatory mechanisms. Front. Cell. Neurosci. 11, 1–19 (2017).
6. Du, C., Collins, W., Cantley, W., Sood, D. & Kaplan, D. L. Tutorials for Electrophysiological Recordings in Neuronal Tissue Engineering. ACS Biomater. Sci. Eng. 3, 2235–2246 (2017).
7. Tsantoulas, C. & McMahon, S. B. Opening paths to novel analgesics: The role of potassium channels in chronic pain. Trends Neurosci. 37, 146–158 (2014).
8. Clare, J. J., Tate, S. N., Nobbs, M. & Romanos, M. A. Voltage-Gated Sodium Channels as Therapeutic Targets. Drug Discov. Today 5, 506–520 (2012).
9. Catterall, W. A., Goldin, A. L. & Waxman, S. G. International Union of Pharmacology. XLIX. Nomenclature and structure-function relationships of voltage-gated sodium channels. Pharmacol. Rev. 57, 397–409 (2005).
10. Burbidge, S. A. et al. Molecular cloning, distribution and functional analysis of the NAV1.6. Voltage-gated sodium channel from human brain. Mol. Brain Res. 103, 80–90 (2002).